Application of a Magnetic SMA Constitutive Model in the Analysis of Magnetomechanical Boundary Value Problems

Björn Kiefer[a] and Dimitris C. Lagoudas[a]

[a] Department of Aerospace Engineering, Texas A&M University, H. R. Bright Building, 3141 TAMU, College Station, TX 77843-3141 USA.

ABSTRACT

A major complication in measuring material properties of ferromagnetic materials is the influence of the demagnetization effect. The resulting difference between the internal and applied magnetic field depends on the specimen geometry and the distribution of the magnetization inside the sample. This phenomenon also affects the interpretability of magnetic-field induced strain and magnetization data measured for magnetic shape memory alloys, which in turn makes the formulation of reliable constitutive models for these materials difficult. To solve this problem, the approximation of uniform magnetization is usually adopted, in which case a tabularized demagnetization factor can be used to correct the data. In this paper, the validity of this simplification is tested by explicitly solving the magnetostatic problem for relevant geometries, while taking the nonuniform magnetization of a magnetic shape memory alloy specimen into account. In addition to comparing the relation between the volume averaged internal and applied magnetic field, the local variation of the magnetic field and magnetization is analyzed.

Keywords: magnetic shape memory alloys, magnetic shape memory effect, magnetic field-induced strain, martensitic variant reorientation, magnetostatics, demagnetization effect.

1. INTRODUCTION

Magnetic shape memory alloys (MSMAs) have recently drawn considerable research[1–7] interest due to their ability to produce magnetic field-induced strains (MFIS) at least one order of magnitude higher than those of ordinary magnetostrictive or piezomagnetic materials. The magnetic shape memory effect (MSME) is a result of the rearrangement of martensitic variants under the influence of magnetic fields. With comparable actuation strains, MSMA exhibit greater bandwidth than conventional shape memory alloys (SMAs), since their actuation frequency is not limited by heat transfer.

To improve the design of MSMA actuators, which have now become commercially available on a limited scale, it is inevitable that the intrinsic coupling between mechanical and magnetic effects in these materials be addressed. Numerical tools are needed to allow the development process to go beyond trial-and-error techniques involving extensive experimental testing. To this end the following analysis components are needed: i) a reliable constitutive model; ii) experimental data to calibrate the model; iii) the capability to solve relevant magnetomechanical boundary value problems.

This paper addresses all three of these aspects. First the general magnetomechanical boundary value problem is defined in Section 2. In Section 3 the Kiefer and Lagoudas[8] constitutive model is summarized. The constitutive relations complete the formulation of the boundary value problem.

In sections 4 and 5 a specific boundary value problem is solved for a prismatic shape memory alloy specimen in a constant applied field. It is thereby illustrated that the solution of coupled magnetomechanical boundary problems for MSMA is not only of interest in the design stages of an actuator, but also for the acquisition of experimental data on which the modeling is based. The analysis is used to both improve the experiments themselves as well as the interpretation of the experimental data. In this manner the experimental and the modeling efforts are designed to mutually benefit each other, thereby raising the level of accuracy with which magnetic shape memory constitutive behavior can be characterized.

Further author information:
Contact Email: lagoudas@aero.tamu.edu

2. THE MAGNETOMECHANICAL BOUNDARY VALUE PROBLEM

In the following paragraphs basic concepts of magnetostatics in the presence of magnetized matter are summarized to provide the foundation for the analysis of magnetostatic boundary value problems (BVPs) for MSMA materials. For static conditions in stationary bodies and negligible current density, Maxwell's equations in $\mathbb{R}^3$, the space occupied by a magnetized body and the infinite surrounding free space, reduce to[9, 10]

$$\nabla\cdot\mathbf{B} = 0\,, \quad \text{and} \quad \nabla\times\mathbf{H} = \mathbf{0}\,, \quad \text{in } \mathbb{R}^3\,. \tag{1}$$

where $\mathbf{B}$ is the magnetic flux density and $\mathbf{H}$ is the magnetic field strength. These two quantities are related through the constitutive relation $\mathbf{B} = \mu_0(\mathbf{H} + \mathbf{M})$, in which μ_0 is the permeability of free space and $\mathbf{M}$ is the magnetization of a material point in a magnetized body, in this case a magnetic shape memory alloy sample. Eqns. (1) are subject to the jump conditions

$$[\![\mathbf{B}]\!]\cdot\mathbf{n} = 0\,, \quad [\![\mathbf{H}]\!]\times\mathbf{n} = \mathbf{0}\,, \tag{2}$$

on all interfaces, if surface currents are negligible. Accordingly, the normal component of the flux density and the tangential component of the field strength have to be continuous over an interface.

Taking advantage of the specific form of Eqns. (1), the magnetostatic problem is often reformulated, by deriving the magnetic field strength from a scalar potential or the flux density from a vector potential. In the latter case $\mathbf{B} = \nabla\times\mathbf{A}$ identically satisfies the first of equations (1). Using the identity $\nabla\times(\nabla\times\mathbf{A}) = \nabla(\nabla\cdot\mathbf{A}) - \Delta\mathbf{A}$, and the Coulomb gauge $\nabla\cdot\mathbf{A} = 0$, the second equation in (1) takes the form

$$\nabla\times(\mu_0^{-1}\nabla\times\mathbf{A} - \mathbf{M}) = \mathbf{0}\,, \quad \text{or} \quad \Delta\mathbf{A} = -\mu_0\nabla\times\mathbf{M} \quad \text{in } \mathbb{R}^3\,, \tag{3}$$

which is the vector-valued Poisson equation for the magnetic potential $\mathbf{A}$.

As a consequence of the Eqns. (1) and (2), a magnetic body is subjected to the magnetostatic field caused by its own magnetization in such a manner that it tends to demagnetize it. This demagnetization effect has relevance when measuring the magnetization response of magnetic materials, since the resulting difference between the externally applied field and internal magnetic field makes experimental data difficult to interpret. However, for uniformly magnetized bodies, the magnetization can be taken outside the integral representation of the solution to the magnetostatic problem,[11] such that

$$\mathbf{H}(\mathbf{r}) = -\left[\frac{1}{4\pi}\iint\limits_{\partial\Omega}\frac{\mathbf{r}-\mathbf{r}'}{|\mathbf{r}-\mathbf{r}'|^3}\otimes\mathbf{n}'\,\mathrm{d}A'\right]\mathbf{M} = -\mathbf{D}\mathbf{M}\,, \tag{4}$$

where $\mathbf{r}$ is the position at which $\mathbf{H}$ is evaluated in $\mathbb{R}^3$ and $\mathbf{r}'$ the location of a point on the surface $\partial\Omega$, with normal $\mathbf{n}'$, of the region Ω occupied by the magnetized body. $\mathbf{D}$ is the demagnetization tensor, which has the following properties: i) it is independent of position inside an ellipsoidal body; ii) it is diagonal if its eigenvectors are aligned with the symmetry axes of the body; iii) its trace is 1, if evaluated inside the body. The demagnetization factor has been computed and tabularized in the literature for a number of standard geometries and numerical solution schemes have been provided for non-ellipsoidal shapes.[12–16] For uniformly magnetized samples of arbitrary shape, the average internal magnetic field can thus be related to a, in this case assumed constant, applied field with the help of the average demagnetization factor as

$$\langle\mathbf{H}\rangle = \mathbf{H}^{\text{applied}} - \langle\mathbf{D}\rangle\mathbf{M}\,. \tag{5}$$

By definition, the demagnetization factor loses its meaning for bodies with nonuniform magnetization. The magnetization induced in a non-ellipsoidal body by an external field is always inhomogeneous. In this case the internal magnetic field can only be determined by explicitly solving the magnetostatic boundary value problem for the considered geometry.

In addition to the magnetostatic equations, the boundary value problem is governed by the mechanical equations in the form of the conservation of linear and angular momentum for the magnetic continuum[17, 18]

$$\nabla\cdot\boldsymbol{\sigma} + \rho\mathbf{f} + \rho\mathbf{f}^{\mathrm{m}} = \mathbf{0} \qquad \text{in } \Omega\,, \tag{6a}$$

$$\operatorname{skw}\boldsymbol{\sigma} = \rho\mathbf{L}^{\mathrm{m}} \quad \text{in } \Omega\,, \tag{6b}$$

where ρ is the mass density, $\boldsymbol{\sigma}$ the Cauchy stress tensor and $\mathbf{f}$ the body force. The additional body force $\mathbf{f}^{\mathrm{m}}$ and the body couple $\mathbf{L}^{\mathrm{m}}$ are due to the magnetization of the body and with the assumption of static fields acting on nonpolarized stationary magnetic materials they are given by[18]

$$\rho\mathbf{f}^{\mathrm{m}} = \mu_0(\nabla\mathbf{H})\mathbf{M}\,, \quad \text{and} \quad \rho\mathbf{L}^{\mathrm{m}} = \operatorname{skw}(\mu_0\mathbf{M}\otimes\mathbf{H})\,. \tag{7}$$

By defining the Maxwell stress tensor as[10, 18]

$$\boldsymbol{\sigma}^{\mathrm{M}} = \mu_0\mathbf{H}\otimes\mathbf{H} + \mu_0\mathbf{H}\otimes\mathbf{M} - \frac{1}{2}\mu_0(\mathbf{H}\cdot\mathbf{H})\mathbf{I}\,, \tag{8}$$

the equilibrium equations (6) can be rewritten as

$$\nabla\cdot\left(\boldsymbol{\sigma} + \boldsymbol{\sigma}^{\mathrm{M}}\right) + \rho\mathbf{f} = \mathbf{0} \quad \text{in } \Omega\,, \tag{9a}$$

$$\operatorname{skw}\left(\boldsymbol{\sigma} + \boldsymbol{\sigma}^{\mathrm{M}}\right) = \mathbf{0} \quad \text{in } \Omega\,, \tag{9b}$$

subject to the jump conditions

$$\left[\!\left[\boldsymbol{\sigma} + \boldsymbol{\sigma}^{\mathrm{M}}\right]\!\right]\cdot\mathbf{n} \quad \text{on } \partial\Omega\,. \tag{10}$$

The coupling between the mechanical and the magnetostatic problem has several contributions:

1. Constitutive relations: The magnetization in Eqn. (3), for example, is not only a function of the magnetic field, but also the applied stress and the loading history through a set of internal state variables $\boldsymbol{\zeta}$. The relation $\mathbf{M} = \mathbf{M}(\boldsymbol{\sigma}, \mathbf{H}, \boldsymbol{\zeta})$ is provided by the constitutive model to be introduced shortly.
2. Body force and body couples (10), captured through Maxwell's stress tensor (9), introduce magnetic field dependence into the equilibrium equations (9);
3. Coupled boundary conditions (10);
4. Deformations of the body, resulting in changes in the domain Ω, affect the solution of the magnetostatic problem (3).

The remaining equations to complete the formulation of the magnetomechanical boundary value problem for magnetic shape memory alloys are the constitutive relations, which are specified in the following section.

3. THE MSMA CONSTITUTIVE MODEL

A phenomenological model has been proposed by the authors to describe the stress- and magnetic field-induced reorientation of martensitic variants in magnetic shape memory alloys. Since the focus of this paper is on the application of the model in combination with the magnetostatic analysis, only a brief summary shall be given here and the reader is referred to previous publication for more detail.[8, 19, 20] The model is based on the Gibbs free energy function G, in which the Cauchy stress tensor $\boldsymbol{\sigma}$ and the magnetic field strength $\mathbf{H}$ are the independent state variables. The loading history dependence of the constitutive behavior, caused by dissipative effects, is introduced through the evolution of internal state variables. The chosen internal state variables are the variant volume fraction ξ, the magnetic domain volume fraction α and the magnetization rotation angles θ_i. These variables are motivated by experimentally observed changes[21] in the crystallographic and magnetic microstructure. The evolution of magnetic domains, although accounted for in the general framework, will be neglected in this paper.

The specific form of the Gibbs free energy for the Kiefer and Lagoudas model[8] is given by

$$G = \hat{G}(\boldsymbol{\sigma}, \mathbf{H}, \xi, \alpha, \theta_i) = -\frac{1}{2\rho}\,\boldsymbol{\sigma} : \mathcal{S}(\xi)\boldsymbol{\sigma} - \frac{\mu_0}{\rho}\mathbf{M}^{\mathrm{eff}}(\xi, \alpha, \theta_i)\cdot\mathbf{H} + G^{\mathrm{an}}(\xi, \alpha, \theta_i) + G^{\mathrm{mix}}(\xi) + G_0 \;, \tag{11}$$

where $\mathcal{S}$, $\mathbf{M}^{\mathrm{eff}}$ and G^{an} are the effective compliance tensor, magnetization vector and magnetocrystalline anisotropy, respectively. The free energy function (11) is comprised of the elastic strain energy, the Zeeman energy, the magnetocrystalline anisotropy energy, a mixing term and a reference state value. The Zeeman or external field energy aims to align the internal magnetization with the externally applied magnetic field. The magnetocrystalline or short magnetic anisotropy energy can be viewed as the energy stored in the material due to the work done by an applied field in rotating the magnetization away from the magnetic easy axes. The mixing term accounts for the deviation of the total free energy from the assumed weighted average of the individual variant and magnetic domain contributions, due to interactions.

Different combinations of these energy terms have also been included in other constitutive models.[3, 22, 23] Unlike most of these formulations, however, this work is concerned with the influence of dissipative effects on the evolution of thermodynamic states, rather than the minimization of the free energy, which searches for equilibrium points in ideal processes. To the authors' knowledge only Hirsinger and Lexcellent[23] and Faidley et al.,[24] with a modification of an earlier Kiefer and Lagoudas model,[25] have also followed this approach, which has yielded powerful phenomenological models for conventional shape memory alloys.[26]

From the free energy expression (11) the constitutive equations are derived in a thermodynamically consistent manner,[8] such that

$$\boldsymbol{\varepsilon}^{\mathrm{e}} = \boldsymbol{\varepsilon} - \boldsymbol{\varepsilon}^{\mathrm{r}} = -\rho\frac{\partial \hat{G}}{\partial \boldsymbol{\sigma}} \;, \qquad \text{and} \qquad \mathbf{M} = -\frac{\rho}{\mu_0}\frac{\partial \hat{G}}{\partial \mathbf{H}} \;, \tag{12}$$

where an additive decomposition of the total strain into an elastic and a reorientation strain part has been assumed, and the total infinitesimal strain is related to the displacement field by $\boldsymbol{\varepsilon} = \frac{1}{2}(\nabla\mathbf{u} - (\nabla\mathbf{u})^{\mathrm{T}})$. A reduced form of the remaining constitutive model equations are summarized in Table 1 for a typical loading case in which only the components σ_{xx} and H_y are non-zero. The table also lists the relations between model parameters and material constants such as the critical magnetic field values for the activation and termination of the variant reorientation process. Exemplary model predictions of the magnetic field-induced strain and the magnetization response are depicted in Figure 1 for different constant stress levels. This particular prediction is based on model parameters calibrated from data published by Heczko et al. 2003.[2] For more details on these predictions the reader is referred to Kiefer and Lagoudas 2005(a,b).[8, 19]

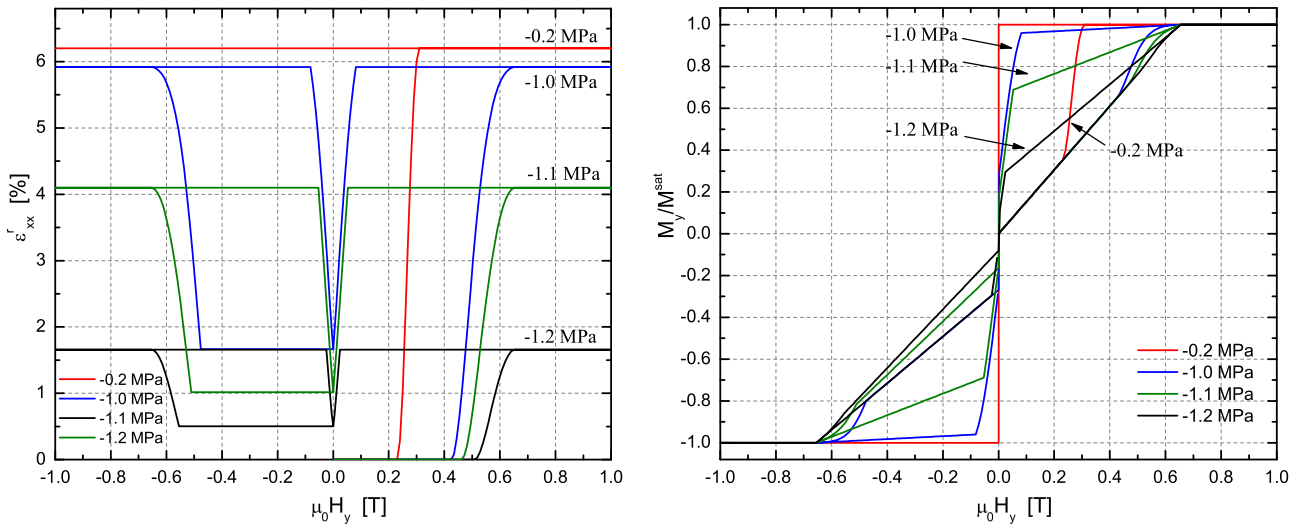

(a) Predicted MFIS hysteresis curves at different stress levels.

(b) Predicted magnetization curves at different stress levels.

Figure 1. Model predictions for the $Ni_{50.7}Mn_{28.4}Ga_{20.9}$ composition, based on Heczko et al. data[2, 19]

Magnetic Field-Induced Strain and Magnetization:

$$\varepsilon^{\mathrm{r}}_{xx} = \varepsilon^{\mathrm{r,max}}\xi \; ; \quad \varepsilon^{\mathrm{r}}_{yy} = -\varepsilon^{\mathrm{r}}_{xx}.$$

$$M_x = (1-\xi)M^{\mathrm{sat}}\sqrt{1-\left(\frac{\mu_0 M^{\mathrm{sat}}}{4\rho K_1}\right)^2 H_y^2} \; ; \quad M_y = \xi M^{\mathrm{sat}} + (1-\xi)M^{\mathrm{sat}}\frac{\mu_0 (M^{\mathrm{sat}})^2}{2\rho K_1}H_y \; .$$

Driving Force for Variant Reorientation:

$$\pi^{\xi} = \sigma_{xx}\Lambda^{\mathrm{r}}_{xx} - \rho\frac{\partial \hat{G}}{\partial \xi} = \sigma\varepsilon^{\mathrm{r,max}} + \mu_0 M^{\mathrm{sat}} H_y - \frac{(\mu_0 M^{\mathrm{sat}})^2}{4\rho K_1}H_y^2 - \frac{\partial f^{\xi}}{\partial \xi} \; .$$

Reorientation Function:

$$\Phi^{\xi}(\boldsymbol{\sigma}, \mathbf{H}, \xi) = \begin{cases} \pi^{\xi} - Y^{\xi,\mathrm{c}} \, , & \dot{\xi} > 0 \\ -\pi^{\xi} - Y^{\xi,\mathrm{c}} \, , & \dot{\xi} < 0 \end{cases} \; .$$

Kuhn-Tucker Loading Conditions:

$$\Phi^{\xi}(\boldsymbol{\sigma}, \mathbf{H}, \xi) \leq 0, \quad \Phi^{\xi}\dot{\xi} = 0 \; .$$

Hardening Function (Derivative):

$$\frac{\partial f^{\xi,\mathrm{c}}}{\partial \xi} = \begin{cases} -A^{\mathrm{c}}\left[\pi - \cos^{-1}(2\xi - 1)\right] + (B_1^{\mathrm{c}} + B_2^{\mathrm{c}}) \, , & \dot{\xi} > 0 \\ -C^{\mathrm{c}}\left[\pi - \cos^{-1}(2\xi - 1)\right] + (B_1^{\mathrm{c}} - B_2^{\mathrm{c}}) \, , & \dot{\xi} < 0 \end{cases} \; .$$

Relations between material constants and model parameters:

$$A^{\mathrm{c}} = \frac{\mu_0 M^{\mathrm{sat}}}{\pi}\left(H_y^{\mathrm{s}(1,2)} - H_y^{\mathrm{f}(1,2)}\right) - \frac{(\mu_0 M^{\mathrm{sat}})^2}{4\pi\rho K_1}\left[\left(H_y^{\mathrm{s}(1,2)}\right)^2 - \left(H_y^{\mathrm{f}(1,2)}\right)^2\right]$$

$$B_1^{\mathrm{c}} = \frac{1}{2}\mu_0 M^{\mathrm{sat}}\left(H_y^{\mathrm{s}(1,2)} + H_y^{\mathrm{f}(2,1)}\right) - \frac{(\mu_0 M^{\mathrm{sat}})^2}{8\rho K_1}\left[\left(H_y^{\mathrm{s}(1,2)}\right)^2 + \left(H_y^{\mathrm{f}(2,1)}\right)^2\right] + \sigma^* \, \varepsilon^{\mathrm{r,max}}$$

$$B_2^{\mathrm{c}} = \frac{\pi}{4}\left(A^{\mathrm{c}} - C^{\mathrm{c}}\right)$$

$$C^{\mathrm{c}} = \frac{\mu_0 M^{\mathrm{sat}}}{\pi}\left(H_y^{\mathrm{f}(2,1)} - H_y^{\mathrm{s}(2,1)}\right) - \frac{(\mu_0 M^{\mathrm{sat}})^2}{4\pi\rho K_1}\left[\left(H_y^{\mathrm{f}(2,1)}\right)^2 - \left(H_y^{\mathrm{s}(2,1)}\right)^2\right]$$

$$Y^{\xi,\mathrm{p}} = \frac{1}{2}\mu_0 M^{\mathrm{sat}}\left(H_y^{\mathrm{s}(1,2)} - H_y^{\mathrm{f}(2,1)}\right) - \frac{(\mu_0 M^{\mathrm{sat}})^2}{8\rho K_1}\left[\left(H_y^{\mathrm{s}(1,2)}\right)^2 - \left(H_y^{\mathrm{f}(2,1)}\right)^2\right] - B_2^{\mathrm{c}}$$

Table 1. Summary of the reduced model equations for the special case of transverse magnetic field and constant axial stress.

4. MAGNETOSTATIC ANALYSIS OF MSMA EXPERIMENTS

As an important example of an application of the magnetomechanical boundary value problem, the influence of the demagnetization effect on the interpretability of MSMA experiments is investigated. As described in the previous section, a typical experiment consists of subjecting a martensitic MSMA sample to a constant mechanical load, which favors one variant, and large shape changes occur when additionally a perpendicular magnetic field is applied to induce the reorientation into another variant. The resulting magnetic field-induced strain and magnetization can only be measured as a function of the applied field. However, to extract the constitutive response that can be used for model calibration, the data needs to be available in terms of the internal magnetic field, which is different from the applied field due to the demagnetization effect, and is not known a priori. The goal therefore is to find the relation between the externally applied and the internal magnetic fields for a MSMA sample of specific geometry, which can then be used to properly interpret the experimental data.

A general discussion of the influence of the demagnetization effect on the measuring of magnetization curves in ferromagnetic materials can be found in O'Handley 2002.[12] Shield[6] addressed the problem for experiments on magnetic shape memory materials by approximating his samples as uniformly magnetized rectangular bars, in which case a constant demagnetization factor according to Eqn. (5) can be utilized. Here, the more general problem of nonuniform magnetization is considered for the following reasons:

1. To take the first step towards solving the fully-coupled boundary value problem;
2. To improve the accuracy with which experimental results can be interpreted. Example: The investigation of the influence of the nonuniformity of the magnetization on the relation between the internal and applied magnetic field;
3. To improve the experiments themselves. Example: The optimal placement of the Hall probe that measures the applied field can be evaluated, if the distribution of the magnetic field around the specimen is known;

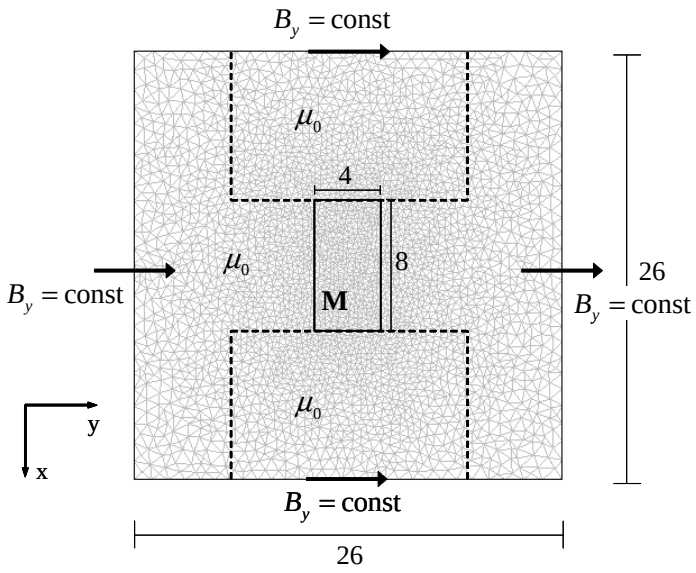

(a) Domain geometry, mesh and boundary conditions for the magnetostatic problem. Dashed lines indicate the location of the nonmagnetic grips of the load frame.

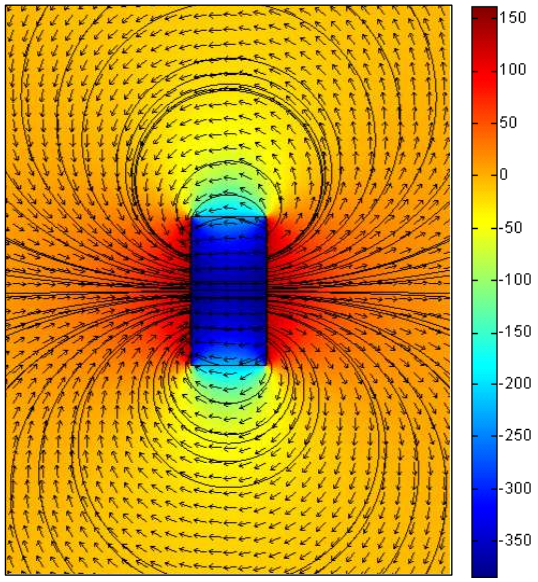

(b) Magnetostatic analysis for uniformly magnetized specimen without an applied magnetic field, and vanishing magnetic potential at infinity. Color surface plot: H_y-component. Arrows and streamlines: Direction of **H**.

Figure 2. Finite element analysis of the 2-D magnetostatic problem.

The geometry of the boundary value problem to be solved is determined by considering typical sample dimensions of 8 mm × 4 mm × 4 mm, or aspect ratios of 2 : 1 : 1, with respect to the axial load direction x, the applied field direction y and the remaining transverse direction z. Due to the numerical complexity of the problem and for illustration purposes, however, the analysis is performed in two-dimensions, which, with an in-plane aspect ratio of 2 : 1, essentially assumes that the specimen extends to infinity in the z-direction. All of the conclusion that will be drawn from this analysis, however, are generalizable to three dimensions. According to electromagnet specification, a uniform magnetic field can be assumed in a gap of the dimensions 26 mm × 26 mm × 26 mm. For the numerical analysis of the magnetostatic problem (3), subject to the jump conditions (2), the finite element mesh depicted in Figure 2(a) is used. This figure also indicates the location of the specimen, and the nonmagnetic grips (dashed lines). A constant magnetic flux of $B_y^{\text{applied}} = \mu_0 H_y^{\text{applied}}$ is applied on the boundary.

All magnetostatic analysis is performed using the COMSOL Multiphysics (FEMLAB) finite element software package. For verification purposes the standard demagnetization factor was computed for a specimen of this

geometry, by solving the magnetostatic problem for a homogeneously magnetized body and applying the condition of a vanishing magnetic potential at infinity (approximated as extending to about five to ten times the dimensions of the specimen). For illustration purposes a section of the solution has been plotted in Figure 2(b). The demagnetization effect is observable in the fact that inside the specimen the magnetic field opposes the direction of the magnetization. It is explained by considering that, to satisfy the relation $\mathbf{B} = \mu_0(\mathbf{H} + \mathbf{M})$ and the interface conditions (2), the magnetic field must jump across the left and right surfaces of the specimen in such a manner that it balances the jump of the magnetization from specimen to surrounding free space, since the normal component of the flux density must be continuous. From integrating the magnetic field over the domain and dividing by the volume and the magnetization, the average demagnetization factor components, cf. Eqn. (5), of

$$\langle D_{xx} \rangle = -\langle H_x \rangle / M_x = 0.355 \ , \quad \text{and} \quad \langle D_{yy} \rangle = -\langle H_y \rangle / M_y = 0.651 \ ,$$

were computed, which will be used for reasons of comparison later.

In order to determine the relation between the applied and the internal magnetic field, without making the assumption of uniformity of the induced magnetization, the following procedure is proposed:

1. Since only a few experimental setups exist in which the MFIS and the magnetization can be measured simultaneously,[2,6] it is assumed that only the MFIS data as a function of the applied magnetic field and stress level is available from experiments. The magnetization curves needed for the analysis are predicted by the constitutive model, cf. Figure 1, which uses the MFIS data for calibration, in addition to the saturation magnetization and the magnetocrystalline anisotropy constant.*

2. The magnetization curves $M_x(H_y)$, $M_y(H_y)$ are used as input to the magnetostatic analysis. The coupling between the mechanical and the magnetic problem in this case exists in the fact that the magnetization curves at different stress levels lead to different solutions of the magnetostatic problem. Magnetic body forces and body couples are neglected, and it is assumed that the changes in geometry due to the magnetic field-induced strains are small enough to be neglected.

3. The problem is solved via finite element analysis. Note that the posed problem is highly nonlinear, since the magnetization on the right hand side of the governing Poisson equation (3) depends on the unknown magnetic potential. With the numerical solution, the relation between internal and applied magnetic fields is established. This relation is used to correct the initially assumed magnetization curves.

4. The magnetostatic problem is solved again with the updated magnetization data as input. This iterative procedure leads to the desired solution of the inverse problem of trying to find the correct internal magnetic field which results in the MFIS vs. applied magnetic field curves measured in the experiment.

Following this procedure, Figure 3(a) depicts the MFIS data used for calibration and the resulting model simulation for a typical experiment. The corresponding magnetization curves shown in Figure 3(b) have been predicted by the constitutive model previously introduced in Section 3. The following assumptions are made for the use of the magnetization data in the finite element analysis: i) To be consistent with the formulation of the model, the effect of the motion of 180° domain walls is neglected, since these are expected to only occur at low magnetic fields. As a consequence the single crystal specimen is initially magnetized in the axial direction even for zero applied field in the transverse direction. The magnetization in the specimen therefore changes only by its rotation and the reorientation of martensitic variants, which is represented by the nonlinearity of the magnetization curve; ii) Even though the x-component of the applied magnetic field is zero, the same does not hold for the internal field, due to the magnetization of the body and the shape of the specimen (corner effects). However, the influence of the x-component of the internal magnetic field on the magnetization is neglected, such that $M_x = M_x(H_y)$ and $M_y = M_y(H_y)$; iii) The hysteretic nature of the constitutive response is not considered in the magnetostatic analysis at this point.

*The former can be found as a function of temperature, for example through Super Quantum Interference Device (SQUID) magnetometer measurements.[20] The magnetocrystalline anisotropy energy ρK_1 can be estimated from the blocking stress, i. e. the stress level at which the applied magnetic field can no longer overcome the stress bias to induce variant reorientation.

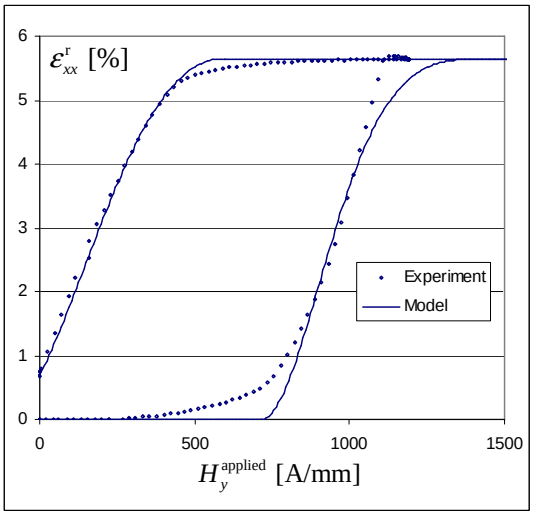

(a) Model calibration. Experimental data (diamonds) and model simulation (solid line). Data taken from Kiefer et al. 2006[20] for a $Ni_{51.1}Mn_{24.0}Ga_{24.9}$ alloy tested at 95 °C under an axial compressive stress of 2 MPa.

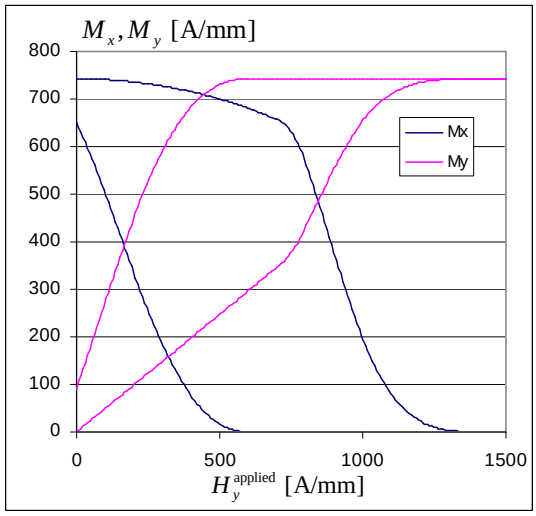

(b) Components of the predicted magnetization curves at −2.0 MPa.

Figure 3. MSMA magnetic field-induced strain and magnetization properties used in the magnetostatic analysis.

The solution of the finite element analysis of the specified nonlinear magnetostatic problem, with all the described assumptions, is plotted in Figure 4 in terms of the change in the distribution of H_y as a function of the applied field. It is observed that indeed, due to the non-ellipsoidal shape of the specimen, the magnetic field and thus the magnetization are nonuniform inside the specimen. Figure 4 also displays the influence of the specimen magnetization on its surroundings, in which the magnetic field without the presence of the specimen would be constant. It is evident from this analysis the Hall probe for measuring the applied field must be placed with care, to minimize the contamination of its readings. The depicted arrows have been added to illustrate the current orientation of the average specimen magnetization. The magnetization, however, changes locally and the local magnetization is comprised of the contributions of both martensitic variants at the scale of the underlying microstructure, whose volume fractions change with the applied field.

To further investigate the local behavior, the variations of the magnetic field and magnetization across and in the neighborhood of the specimen are plotted in Figure 5 for the exemplary applied magnetic field of $H_y^{\text{applied}} = 1034.5\ \text{Amm}^{-1}$. This applied field level is particularly interesting because it falls into the region in which variant reorientation occurs (cf. Figure 3).

5. INTERPRETATION OF THE CONSTITUTIVE RELATIONS

After obtaining the solution to the magnetostatic problem, the next step is to use the relation between the applied and internal magnetic field to reinterpret the experimental magnetic field-induced strain and magnetization curves. As described, this has already been done as part of the iterative procedure of solving the magnetostatic problem, but this important issue shall be discussed here in more detail.

The magnetostatic analysis has been performed in four iterations, each time using the updated data of the last iteration as input for the next. The original and updated MFIS and magnetization curves are depicted in Figure 6. The original MFIS curve corresponds to the experimental data of Figure 3(a), the original magnetization curve to the initial prediction by the constitutive model of Figure 3(b). The updated curves were plotted by always using the same data for the vertical axes, while rescaling the magnetic field axis by means of the relation between the average internal and applied field. One observes that this iterative procedure leads to relatively fast convergence of the desired solution. The inverse problem has therefore successfully been solved, meaning

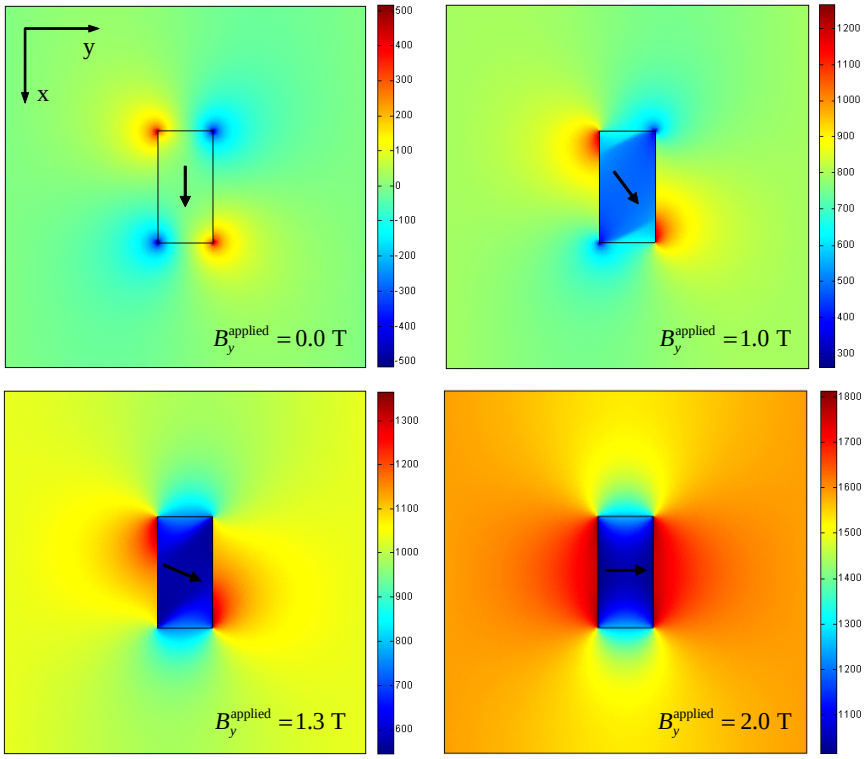

Figure 4. Rotation of the induced magnetization and the associated distribution H_y at $B_y^{\text{applied}} = 0.0\,\text{T}, 1.0\,\text{T}, 1.3\,\text{T}, 2.0\,\text{T}$ (or $H_y^{\text{applied}} = 0.0\,\text{A/mm}, 795.77\,\text{A/mm}, 1034.51\,\text{A/mm}, 1591.55\,\text{A/mm}$). All plots are based on the solution after the final iteration.

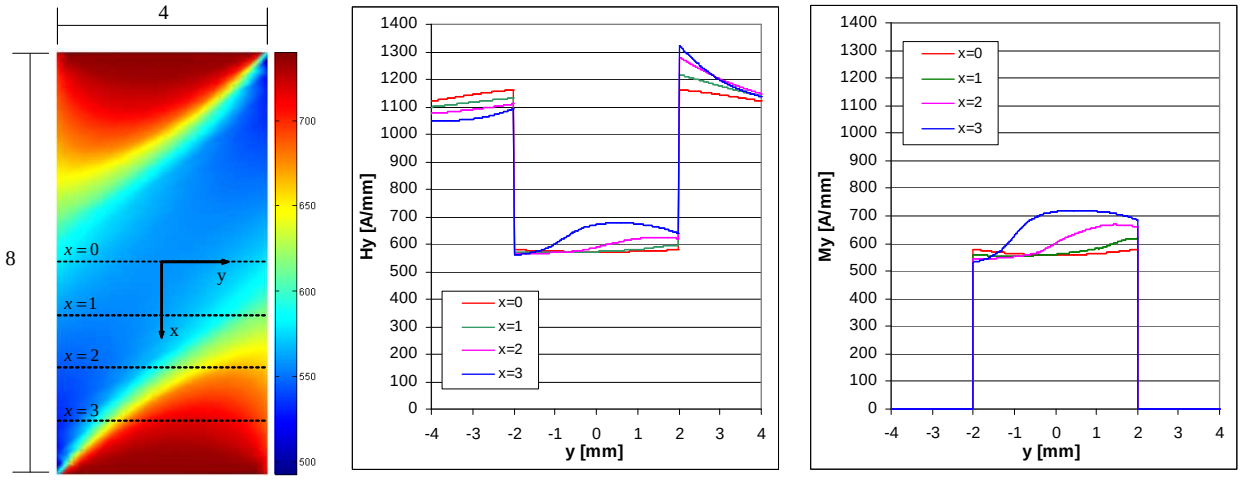

(a) Surface plot of H_y over the specimen.

(b) $H_y(x)$ along lines of constant x.

(c) $M_y(x)$ along lines of constant x.

Figure 5. Distribution of H_y and M_y at $B_y^{\text{applied}} = \mu_0 H_y^{\text{applied}} = 1.3\,\text{T}$ (or $H_y^{\text{applied}} = 1034.5\,\text{Amm}^{-1}$) across the specimen. All plots are based on the solution after the final iteration.

that the correct relation between the internal and applied field has been found, such that when the $M_x(H_y)$ and $M_y(H_y)$ curves are used as the assumed magnetization behavior for solving the magnetostatic problem, the original relation of $M_y(H_y^{\text{applied}})$ is obtained.

The analysis suggests that the simplifying assumption of uniform magnetization and constant shape-dependent

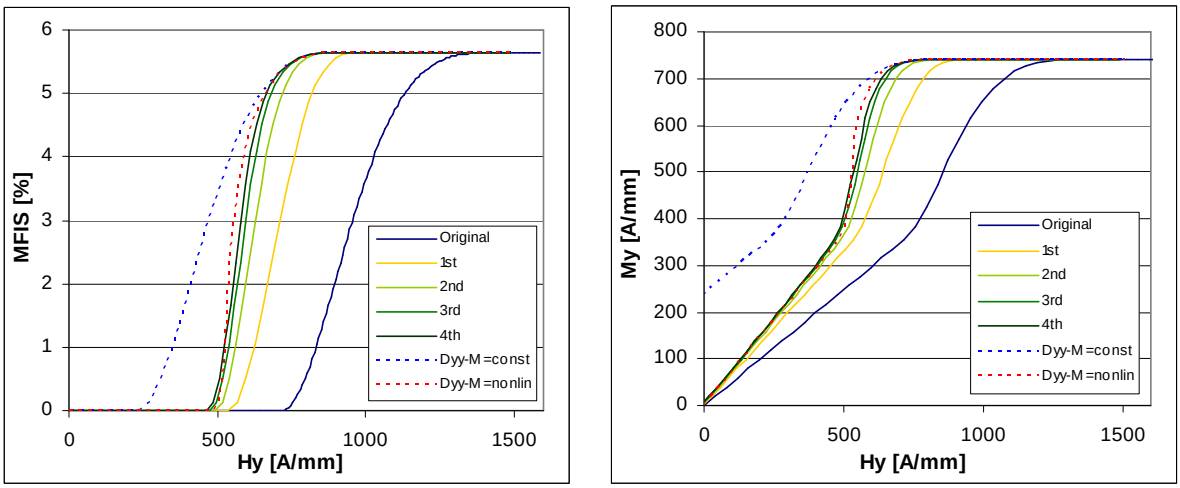

(a) Updated magnetic field-induced strain data.

(b) Updated magnetization data.

Figure 6. MFIS and Magnetization data corrected for demagnetization after four iterations of magnetostatic analysis (solid lines) and using the standard demagnetization factor with constant or nonlinear magnetization curves (dashed lines).

demagnetization factor (dashed red line in Figure 6), leads to essentially the same result as using the average of the solution with nonuniform magnetization (solid dark green line), if the correct nonlinear variation of the magnetization is considered. If the magnetization curves are not known from experiments and are also not predicted by a constitutive model, the only choice is to assume a constant magnetization with the magnitude of the saturation magnetization, which, with the same demagnetization factor, does not lead to a satisfactory prediction, as evident from Figure 6 (dashed blue line).

However, the difference of local and volume averaged fields can be very large. To show this the variation of the internal magnetic field as a function of location and applied field is considered. Figure 7 displays the relative difference of the local field from the volume average at several points in the specimen.[†] For problems in which the knowledge of local magnetic field and magnetization is important, solving the magnetostatic problem explicitly, as performed here, is inevitable. Such cases are certainly encountered if one is interested in solving magnetomechanical MSMA boundary value problems not just involving simple specimen shapes, but for example geometries of active components in actuators.

6. DISCUSSION

The main results of the work presented in this paper can be summarized as follows:

- The fully-coupled magnetomechanical boundary value problem involving magnetic shape memory alloy constitutive behavior was formulated.
- As an exemplary application, the demagnetization effect in MSMA specimen was investigated. Numerical solutions have shown the influence of shape and nonuniformity of the magnetization on the relation between the internal and applied magnetic field, which has an implication on the interpretation of material response measurements.
- For the averaged field variables it was found that demagnetization factors, which assume a uniform induced magnetization in the specimen, lead to a good approximation of the demagnetization effect, if the correct nonlinear magnetization curves are utilized. However, the local fields and the resulting change in the local magnetization greatly deviate from their volume averages.

[†]The values are only plotted for fields larger than 300A/mm, since for small fields the relative differences are very large. Furthermore, at higher fields one can assume that the influence of the neglected domain wall motion does not contaminate the result.

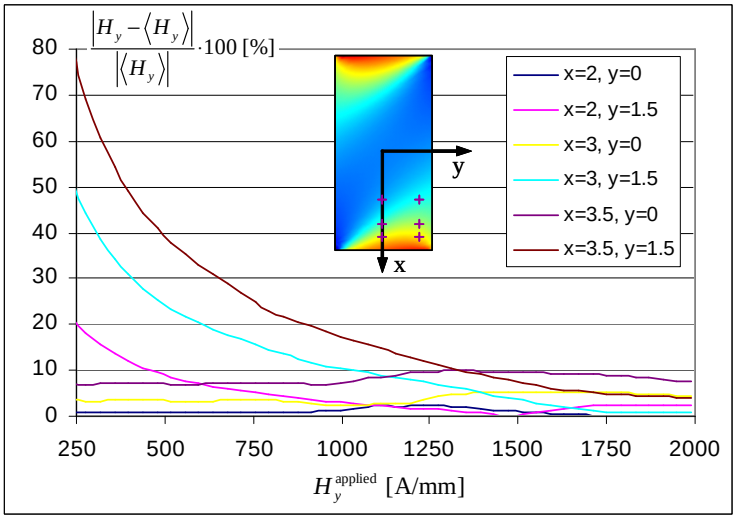

Figure 7. Relative difference in local and average H_y at different locations (crosses) of the specimen vs. applied magnetic field. All plots are based on the solution after the first iteration.

- Due to the complexity of the analysis, the magnetostatic problem has only been investigated for the special case of a prismatic $Ni_{51.1}Mn_{24.0}Ga_{24.9}$ specimen under an applied stress of $-2\,\text{MPa}$, subjected to a transverse applied magnetic field of up to $2\,\text{T}$. However, the methods introduced here are general and can be employed to investigate many problems of interest in the characterization of magnetic shape memory alloys. The magnetostatic analysis is not limited to the study of the demagnetization effect, but can for example be used to analyze boundary value problems of interest in MSMA actuator design.

In future work the following issues will be addressed:

- Solution of the 3-D coupled magnetostatic problem.
- From the analysis presented in this paper, it is evident that material points inside the specimen will, in general, not exclusively be exposed to transverse components of the magnetic field, as assumed in the reduction of the constitutive model equations. The influence of complex multiaxial mechanical and magnetic loading needs to be addressed.[27]
- As the ultimate goal the fully-coupled magnetomechanical boundary value problem for MSMA defined in Sections 2 and 3 is to be solved.

ACKNOWLEDGMENTS

This work was supported by the Army Research Office, contract no. DAAD 19-02-1-0261 and the National Science Foundation, award no. CMS-0324537. The authors would also like to thank Ms. Alicia Broederdorf for her support in conducting the finite element analysis.

REFERENCES

1. T. Yamamoto, M. Taya, Y. Sutou, Y. Liang, T. Wada, and L. Sorensen, "Magnetic field-induced reversible variant rearrangement in Fe-Pd single crystals," *Acta Materialia* **52**(17), pp. 5083–5091, 2004.
2. O. Heczko, L. Straka, and K. Ullakko, "Relation between structure, magnetization process and magnetic shape memory effect of various martensites occuring in Ni-Mn-Ga alloys," *Journal de Physique IV France* **112**, pp. 959–962, 2003.
3. R. C. O'Handley, "Model for strain and magnetization in magnetic shape-memory alloys," *Journal of Applied Physics* **83**(6), pp. 3263–3270, 1998.

4. S. J. Murray, M. Marioni, P. G. Tello, S. M. Allen, and R. C. O'Handley, "Giant magnetic-field-induced strain in Ni-Mn-Ga crystals: Experimental results and modeling," *Journal of Magnetism and Magnetic Materials* **226–230**(1), pp. 945–947, 2001.
5. P. Müllner, V. A. Chernenko, and G. Kostorz, "A microscopic approach to the magnetic-field-induced deformation of martensite (magnetoplasticity)," *Journal of Magnetism and Magnetic Materials* **267**, pp. 325–334, 2003.
6. T. W. Shield, "Magnetomechanical testing machine for ferromagnetic shape-memory alloys," *Review of Scientific Instruments* **74**(9), pp. 4077–4088, 2003.
7. A. A. Likhachev, A. Sozinov, and K. Ullakko, "Different modeling concepts of magnetic shape memory and their comparison with some experimental results obtained in Ni-Mn-Ga," *Material Science & Engineering A* **378**, pp. 513–518, 2004.
8. B. Kiefer and D. C. Lagoudas, "Magnetic field-induced martensitic variant reorientation in magnetic shape memory alloys," *Philosophical Magazine Special Issue: Recent Advances in Theoretical Mechanics, in Honor of SES 2003 A.C. Eringen Medalist G.A. Maugin* **85**(33-35), pp. 4289–4329, 2005.
9. J. D. Jackson, *Classical Electrodynamics*, John Wiley & Sons, 2nd ed., 1975.
10. H. H. Woodson and J. R. Melcher, *Electromechanical Dynamics, Part I: Discrete Systems*, Krieger Publishing Company, Reprint of 1968 ed., 1990.
11. H. N. Bertram, *Theory of Magnetic Recording*, Cambridge University Press, 1994.
12. R. C. O'Handley, *Modern Magnetic Materials*, John Wiley & Sons, 2000.
13. B. D. Cullity, *Introduction to Magnetic Materials*, Addison-Wesley, 1972.
14. R. M. Bozorth, *Ferromagnetism*, IEEE Press, reissue of 1951 ed., 1993.
15. E. Schlömann, "A sum rule concerning the inhomogeneous demagnetizing field in nonellipsoidal samples," *Journal of Applied Physics* **33**(9), pp. 2825–2826, 1962.
16. R. Moskowitz and E. Della Torre, "Theoretical aspects of demagnetization tensors," *IEEE Transactions on Magnetics* **2**(4), pp. 739–744, 1966.
17. A. C. Eringen and G. A. Maugin, *Electrodynamics of Continua I — Foundations and Solid Media*, Springer-Verlag, 1990.
18. K. Hutter and A. A. F. van de Ven, *Field Matter Interactions in Thermoelastic Solids*, vol. 88 of *Lecture Notes in Physics*, Springer-Verlag, 1978.
19. B. Kiefer and D. C. Lagoudas, "Modeling of the magnetic field-induced martensitic variant reorientation and the associated magnetic shape memory effect in MSMAs," *Proceedings of SPIE, Smart Structures and Materials: Active Materials: Behavior and Mechanics, San Diego, CA, 6–10 March 2005* **5761**, pp. 454–465, 2005.
20. B. Kiefer, H. E. Karaca, D. C. Lagoudas, and I. Karaman, "Characterization and modeling of the magnetic field-induced strain and work output in Ni_2MnGa shape memory alloys," *Submitted to Journal of Magnetism and Magnetic Materials* , 2005.
21. M. R. Sullivan and H. D. Chopra, "Temperature- and field-dependent evolution of micromagnetic structure in ferromagnetic shape-memory-alloys," *Physical Review B* **70**, pp. 094427–(1–8), 2004.
22. R. D. James and K. F. Hane, "Martensitic transformations and shape-memory materials," *Acta Materialia* **48**(1), pp. 197–222, 2000.
23. L. Hirsinger and C. Lexcellent, "Internal variable model for magneto-mechanical behaviour of ferromagnetic shape memory alloys Ni-Mn-Ga," *Journal de Physique IV France* **112**, pp. 977–980, 2003.
24. L. E. Faidley, M. J. Dapino, G. N. Washington, and T. A. Lograsso, "Reversible strain in Ni-MnGa with collinear field and stress," *Proceedings of SPIE, Smart Structures and Materials: Active Materials: Behavior and Mechanics, San Diego, CA, 6–10 March 2005.* **Vol. 5761**, 2005.
25. B. Kiefer and D. C. Lagoudas, "Phenomenological modeling of ferromagnetic shape memory alloys," *Proceedings of SPIE, Smart Structures and Materials: Active Materials: Behavior and Mechanics, San Diego, CA, 14–18 March 2004* **5387**, pp. 164–176, 2004.
26. D. C. Lagoudas, P. B. Entchev, P. Popov, E. Patoor, L. C. Brinson, and X. Gao, "Shape memory alloys, Part II: Modeling of polycrystals," *Mechanics of Materials* **38**, pp. 430–462, 2006.
27. B. Kiefer and D. C. Lagoudas, "Modeling the reorientation in magnetic shape memory alloys subject to complex magnetomechanical loading," *Not yet published* , 2006.